THE ASTROPHYSICAL JOURNAL, 558:693–701, 2001 September 10

SMALL-SCALE ABUNDANCE VARIATIONS IN TMC-1: DYNAMICS AND HYDROCARBON CHEMISTRY

J. E. DICKENS, W. D. LANGER, AND T. VELUSAMY
Jet Propulsion Laboratory, 4800 Oak Grove Drive, MS 169-506, California Institute of Technology, Pasadena, CA 91109-8099;
james.dickens@jpl.nasa.gov, william.langer@jpl.nasa.gov, velu@rams.jpl.nasa.gov
Received 2001 February 22; accepted 2001 May 10

ABSTRACT

We present high spectral resolution observations of eighteen molecules, including high-quality maps of CCS and HC_7N in TMC-1, using NASA's Deep Space Network 70 m antenna to study the interaction between cloud dynamics and chemistry. Other molecules shown in our study are $C^{18}O$, NH_3, CS, C_3S, C_3H_2, H_2C_3, H_2C_4, H_2C_6, HC_3N, HC_5N, DC_5N, HC_9N, C_4H, C_5H, C_6H, and a successful detection of the rare C_8H molecule. In addition, we have searched for and set meaningful abundance limits on several carbon chain and ring molecules such as C_7H, H_2C_5, c-H_2C_5, and biogenic molecules such as pyrrole and glycine. All the species observed in TMC-1 show large spectral-line variations in both intensity and shape over extremely small scales ($\sim$0.03 pc). Maps of CCS and HC_7N display abundance ratio variations of 3–5 along individual lines of sight. The high degree of clumpiness, transient nature of clumps, and gas-phase enrichment adequately explain the "early-time" chemistry and the molecular complexity in TMC-1. This enrichment has interesting implications for hydrocarbon chemistry in TMC-1, and presumably other clumpy, dark clouds. Specifically, the large number of clumps at various stages of early-time chemical evolution increases the chances for detection of complex hydrocarbons, since the probability of observing a clump at the time of peak abundance for a given molecular species is increased. We suggest two mechanisms for explaining the small-scale variations: (1) the passage of MHD waves in a clumpy medium and (2) grain impacts during clump-clump collisions. In the quiescent region far from any protostar, the MHD activity can be generated locally by clump collisions. The passage of MHD waves helps maintain early-time chemistry in the clumps. Both mechanisms provide enough energy to raise grain temperatures from 10 K to $T_{crit} \sim 30$ K, sufficient to cause reactive radical explosions in grain mantles and thermal desorption. In this manner, the mantle injection causes TMC-1 to exhibit some aspects of "hot-core" chemistry, as seen in more massive star-forming regions. The transient nature of the clumps and the mantle-driven chemistry make TMC-1 a good target for future searches of complex molecular species.

Subject headings: astrochemistry — ISM: clouds — ISM: individual (TMC-1) — ISM: molecules — radio lines: ISM

1. INTRODUCTION

Molecular cloud cores in dark clouds are important sites of future low-mass star formation. Little is known about the precollapse phases of star formation (when stable cores form and evolve as distinct dynamical units) and their chemistry. Only a few sources are known to trace this stage of core evolution. Some examples are L1498 (Kuiper, Langer, & Velusamy 1996; Willacy, Langer, & Velusamy 1998), L1544 (Caselli et al. 1999; Ohashi et al. 1999), sources in NGC 1333 (Lefloch et al. 1998), and sources in ρ Oph (Mezger et al. 1992). One of the most promising regions for understanding the formation of cores and their chemical history is the Taurus molecular complex (TMC), and especially the quiescent region TMC-1. Here we study the small-scale structural components within TMC-1 to understand the chemical and dynamical state of prestellar core formation.

Several recent studies have focused on the small-scale structure of TMC-1 (Langer et al. 1995; Wolkovitch et al. 1997; Peng et al. 1998). Peng et al. (1998) identified 45 dense clumps traced by CCS toward core D in TMC-1 in the regime of 0.02–0.04 pc and 0.04–0.6 $M_\odot$. In that study, they determined that these clumps were more likely to further fragment or merge because of collisions with other clumps as they moved through the dense ridge, rather than remain intact. The clump-clump collisions could be a common occurrence. Collisions between clumps could have an effect on their chemistry via rapid injection of grain material into the gas phase by the passage of MHD waves generated during clump collisions (Markwick, Millar, & Charnley 2000). It has already been suggested for TMC-1 that large-scale chemical abundance gradients trace the dynamics of the dense ridge (Pratap et al. 1997; Hirahara et al. 1992; Bergin, Snell, & Goldsmith 1996; van Dishoeck et al. 1993). Here we investigate small-scale clump dynamics and their effect on the chemistry.

The purpose of this study is (1) to determine the degree of complexity of the molecular species in TMC-1 by searching for new molecules, (2) to trace the small-scale structure using several dense-gas tracers, (3) to analyze the abundance gradients using tracer molecules such as HC_7N and CCS for clues to the dynamical state, and (4) to interpret the chemical complexity in terms of gas-phase, gas-grain, and grain-grain processes. Mechanisms for grain-mantle removal and production of rich organic species make TMC-1 an ideal target for complex molecule searches.

2. OBSERVATIONS

The observations were made with NASA's Deep Space Network (DSN) 70 m antenna at Goldstone, CA, over a period of time from 1996 to 1998. Observations toward one position in TMC-1 were made of the complex carbon species C_7H, C_8H, H_2C_5, and c-C_5H_2, the biogenic species pyrrole (c-C_4H_5N), and the lowest energy conformer of

TABLE 1

MOLECULAR TRANSITIONS OBSERVED IN TMC-1

Species	Transition	Frequency (MHz)
C_7H	$J = 12.5 \rightarrow 11.5$	21862.88/21862.92
C_8H	$J = 19.5 \rightarrow 18.5$	22879.91/22880.12
H_2C_5	$4(1, 3) \rightarrow 3(1, 2)$	18399.92
H_2C_5	$5(1, 5) \rightarrow 4(1, 4)$	22904.98
c-C_5H_2	$3(1, 3) \rightarrow 2(1, 2)$	19588.72
c-C_5H_2	$3(0, 3) \rightarrow 2(0, 2)$	20107.80
pyrrole[a]	$2(0, 2) \rightarrow 1(0, 1)$	22724.37
glycine-I[b].....	$3(1, 2) \rightarrow 2(1, 1)$	21745.18

[a] Pyrrole (c-C_4H_5N).
[b] Glycine-I (NH_2CH_2COOH).

glycine (glycine-I, NH_2CH_2COOH). These observations were made as part of a continuing effort to study the chemistry and structure in TMC-1 (Langer et al. 1995, 1997; Peng et al. 1998). The frequencies and transitions observed are included in Table 1. These species were observed toward the position R.A.(1950.0) = $04^h38^m41^s.0$, decl.(1950.0) = 25°35′40″, and were made in frequency-switching mode using a local oscillator (LO) offset of 0.5 MHz.

In addition, the emission from the HC_7N ($J = 20 \rightarrow 19$) transition at 22,559.9 MHz was mapped with high spectral resolution (0.008 km s^{-1}) and an excellent signal-to-noise ratio over a 4′ × 4′ region centered on R.A.(1950.0) = $04^h38^m39^s.0$, decl.(1950.0) = 25°35′30″. This center position was approximately 1′ southwest of the cyanopolyyne peak in the core D region of the observation by Hirahara et al. (1992). The FWHM antenna beam was 45″, and the map was sampled every 25″, such that it was nearly Nyquist sampled. The observations were made in position-switching mode with a 30′ offset in azimuth to suppress any effects caused by elevation changes. The integration time for the on-off pair was 10 minutes.

All observations were made with a broadband (17.5–26.5 GHz) cooled *K*-band high electron mobility transistor (HEMT) receiver with typical system temperatures of ~55–70 K at 22 GHz, depending on weather and elevation. Calibration of the antenna temperature was made for each observation with a noise diode and an ambient load. The main beam efficiency was estimated to be 70% for extended sources (Langer et al. 1995) and 45% for point sources. The back end consisted of a two million channel wide band spectrum analyzer (WBSA) with a spectral resolution of 19 Hz over 40 MHz. The resolution was reduced by co-adding 32 adjacent channels together to provide 610 Hz resolution (0.008 km s^{-1} at 22 GHz). For all but HC_7N, the spectral resolution was further smoothed to 0.05 km s^{-1} for signal-to-noise ratio improvement.

3. RESULTS

3.1. *Complex Carbon Molecules*

Many earlier studies have presented evidence for at least three velocity components in TMC-1 spectra for many molecular species (Langer et al. 1995, 1997; Pratap et al. 1997; Peng et al. 1998). Figure 1 shows a panel of spectra for 18 molecules, ranging from structures as simple as $C^{18}O$, NH_3, and CS, to as complex as HC_9N, and as rare as DC_5N and C_8H, taken toward the position R.A.(1950.0) = $04^h38^m41^s.0$, decl.(1950.0) = 25°35′40″ in TMC-1. The three prominent velocity components occur at 5.7, 5.9, and 6.1 km s^{-1}. These velocity features have previously been analyzed as distinct physical structures from CCS data (Peng et al. 1998). The differences in spectral shapes for a variety of molecular species reveal a complex chemical structure in these clumps as well (Fig. 1).

If we assume that species with similar structures but successively more carbon share similar formation and destruction pathways, then we expect these related species to trace the same gas and have comparable spectral shapes. This expectation is not realized for the species in Figure 1. Take, for example, the species based on the CS backbone, C_nS ($n = 1, 2, 3$). The CS and CCS spectra have stronger intensities near 5.7 km s^{-1}, while C_3S is strongest at higher velocities. While CS may suffer from opacity effects, CCS and C_3S are more likely to be optically thin. For the latter species, the chemical abundance scales directly with intensity. Therefore, C_3S is more abundant at larger velocities than CCS toward this line of sight. We see similar results for the other backbone families, H_2C_n ($n = 3, 4, 6$), H/DC_nN ($n = 3, 5, 7, 9$), and C_nH ($n = 4, 5, 6, 8$). Given that the more complex carbon chains are predicted to peak at a slightly later time in the evolution of a core, we believe that these distinct velocity structures represent clumps in close proximity with different evolutionary status.

Six other molecular carbon chains were observed toward this same position in TMC-1 (see Table 1) for the purpose of expanding previous studies of complex carbon species (Langer et al. 1995). Of these species, only C_8H was detected. Although this detection is being included here as part of this study, it was first reported in 1997 at the Exobiology Conference (Velusamy, Langer, & Levin 1998). The observation was made in 1996 November, making it the first detection of the C_8H radical in a cold interstellar cloud core (Fig. 2). An independent detection was made by Bell et al. (1999).

The C_8H column density is calculated using the relationship between integrated intensity and column density in Turner (1991, see his Appendix A), assuming that the emission is optically thin and that the energy levels are populated according to a Boltzmann distribution with a temperature of 5 K, similar to other complex molecules in TMC-1 (Pratap et al. 1997). For the nondetected species, we calculate upper limits to the integrated intensity by using 3 times the baseline rms as the peak temperature and assuming a line width of 0.15 km s^{-1}, consistent with that found for C_8H in this study. The 3 σ upper limit to the column density is then calculated using the relationship between integrated intensity and column density (Turner 1991). The column density results are shown in Table 2.

3.2. *Searches for Biogenic Molecules*

The evidence for physical and chemical complexity in TMC-1 and the development of more sensitive receivers prompted a renewed search for two important biogenic species, pyrrole (c-C_4H_5N) and the lowest energy conformer of glycine (glycine-I, NH_2CH_2COOH). Pyrrole is a cyclic species that is an important structural component of chlorophyll and hemoglobin. Glycine is the simplest amino acid, and it has been targeted for searches of biogenic species because of its simplicity compared to other amino acids. Amino acids have been detected in meteorites (Cronin &

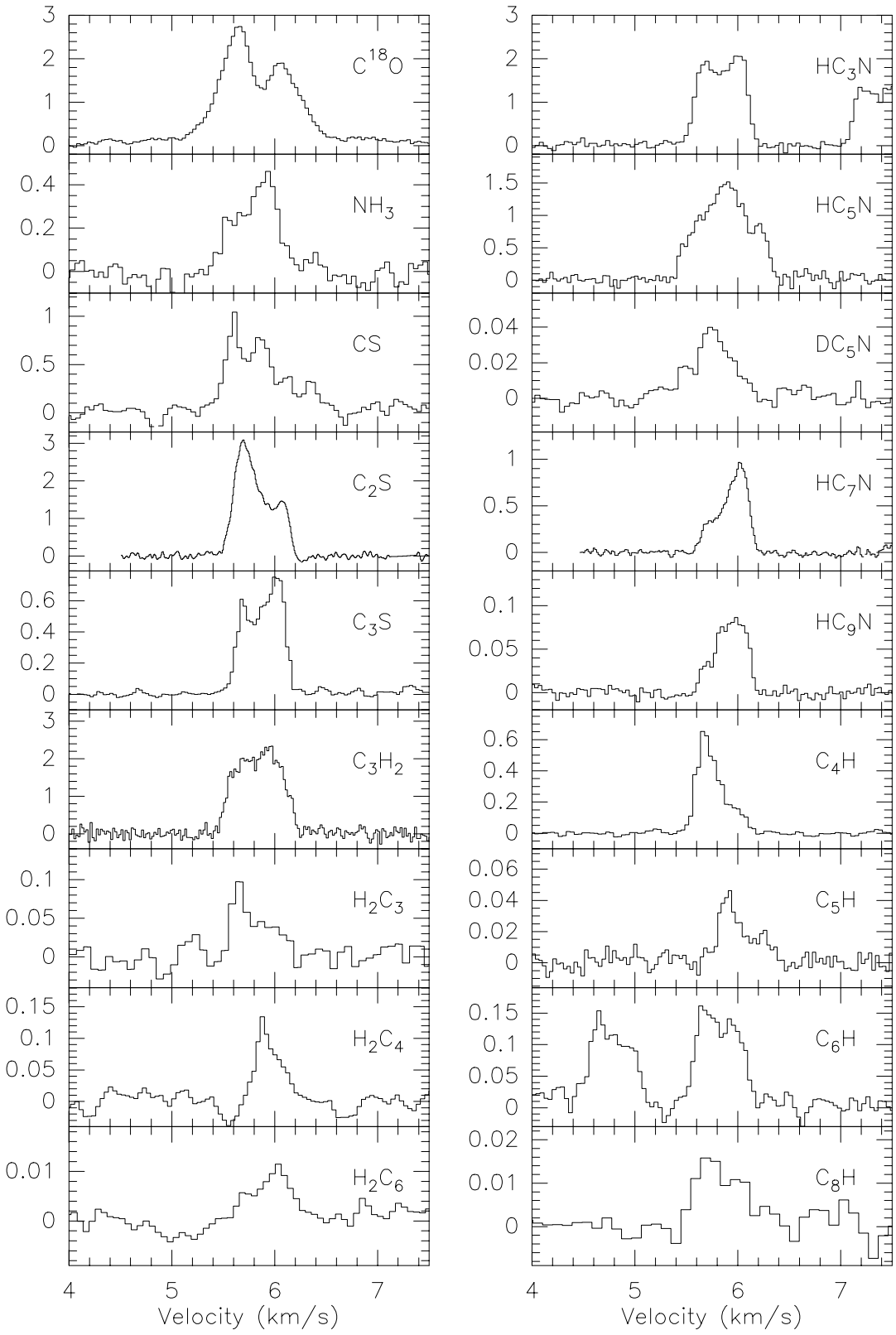

FIG. 1.—Spectra of TMC-1 toward the position R.A.(1950.0) = $04^{h}38^{m}41\overset{s}{.}0$, decl.(1950.0) = 25°35′40″, taken with the NASA/DSN 70 m antenna. Note the three velocity components at 5.7, 5.9, and 6.1 km s^{-1}. Also, for each of the carbon chain families [C_nS (n = 1, 2, 3), H_2C_n (n = 3, 4, 6), $H(D)C_nN$ (n = 3, 5, 7, 9), and C_nH (n = 4, 5, 6, 8)], there are large emission differences among the three velocity components, suggesting small-scale chemical abundance variations in a clumpy medium.

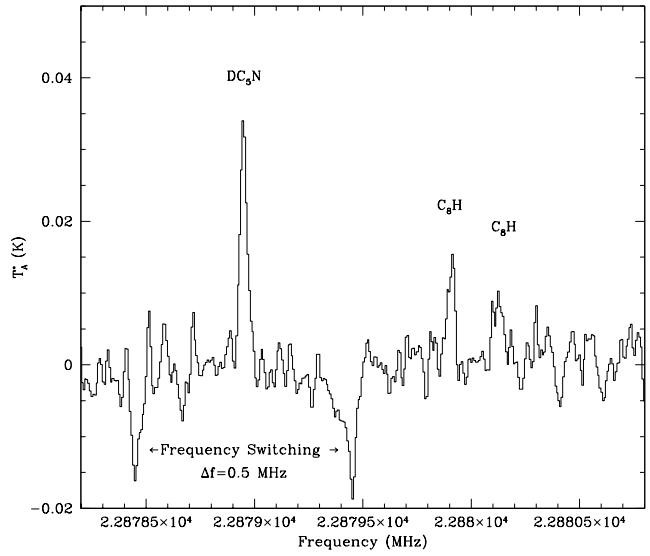

FIG. 2.—Observed C_8H spectrum in TMC-1 toward the position R.A.(1950.0) = $04^h38^m41^s0$, decl.(1950.0) = 25°35′40″. The spectral resolution was 0.008 km s^{-1}, and has been smoothed to 0.024 km s^{-1}. This was the first detection of the C_8H radical in a cold interstellar cloud core (first reported by Velusamy et al. 1998 and Velusamy & Langer 1998); an independent reporting was made by Bell et al. (1999). The DC_5N line attests to the high sensitivity of the *K*-band receiver at the DSN.

Chang 1993). Therefore, detection of an amino acid in interstellar clouds similar to that from which our solar nebula emerged would make an appealing scenario for an extrasolar origin of the materials needed for the origin of life.

Neither species was detected. However, our upper limit for pyrrole is nearly an order of magnitude lower than that obtained by previous searches in TMC-1 (Kutner et al. 1980; Myers, Thaddeus, & Linke 1980). Although few search attempts have been made for glycine in a cold, dense cloud, our upper limit to the abundance relative to H_2 is as sensitive as that just reported in the solar-type protostar IRAS 16293-2422, where $N(\text{glycine-I}) < 10^{11}$ cm^{-2} (Ceccarelli et al. 2000). Future searches will require much more sensitive receivers that are stable enough to attain sub-mK rms noise levels. However, the clumpy nature, the narrow line widths, and the complex hydrocarbon chemistry make TMC-1 an ideal target for future searches of such complex molecular species.

3.3. HC_7N *and* CCS *Maps*

The large dipole moment of HC_7N (~5.0 D) makes it a good tracer of the densest gas along the line of sight. This property allows us to compare its emission with that of another dense-gas tracer, CCS, which has been mapped and analyzed previously by Peng et al. (1998) in the same region with the same spatial and spectral resolution. Both CCS and HC_7N have narrow thermal line widths (~0.1 km s^{-1} at 10 K), such that we are able to reliably disentangle the complex velocity structure in TMC-1.

Figure 3 shows the integrated intensity maps for CCS (*gray scale*) and HC_7N (*contours*) toward TMC-1 in three different velocity ranges. The CCS map has been discussed at length by Peng et al. (1998). The most important features that were noted in that analysis were the elongated ridge running southeast to northwest, similar to other carbon species in TMC-1 (Olano, Walmsley, & Wilson 1988; Hirahara et al. 1992; Pratap et al. 1997), and the extremely clumpy nature of the emission. HC_7N also appears to trace the ridge of dense gas. However, the emission peaks of HC_7N do not coincide with those of CCS. This difference is most apparent in the lowest velocity frame (5.50–5.75 km s^{-1}), in which the HC_7N emission peaks approximately 1′ north of the CCS peak. In the source rest-frame map (5.75–6.00 km s^{-1}), there are two peaks in the HC_7N emission on either side of a CCS minimum. Toward the southeastern end of the ridge, the CCS peaks as the HC_7N emission falls off. Even at the highest velocities (6.00–6.25 km s^{-1}), the HC_7N emission peaks 30″ west of the strongest CCS emission. These results imply chemical variations on the order of our beam size, 45″, or 0.03 pc at the distance of TMC-1 (140 pc).

To separate the small-scale structures along the line of sight, we have fitted multiple Gaussian components to the observed spectral line profiles. Following the approach described by Peng et al. (1998), we fit the two outer velocity components first, and then fit a third Gaussian to the residual. The fitted profiles toward two positions are given in Figure 4, and the fitted Gaussian parameters are shown in Table 3. The line widths for each component are in the range 0.14–0.19 km s^{-1} for both species, compared to 0.07 km s^{-1} and 0.09 km s^{-1} for the thermal broadening of HC_7N and CCS, respectively, at 10 K. We calculate that any nonthermal component of the line width is at most 0.12–0.17 km s^{-1}. Since the thermal broadening of H_2 is approximately 0.4 km s^{-1} at 10 K, then the nonthermal

TABLE 2

OTHER SPECIES SEARCHES IN TMC-1

Species	Transition	T_A^* (mK)	ΔV (km s^{-1})	N(species) (cm^{-2})	X(species)
C_7H	$J = 12.5 \rightarrow 11.5$	<5	0.15[a]	<4.0E11	<2.0E−11
C_8H	$J = 19.5 \rightarrow 18.5$	12/10	0.15	3.0E11	1.5E−11
H_2C_5	4(1, 3) → 3(1, 2)	<3	0.15[a]	<1.0E12	<5.0E−11
H_2C_5	5(1, 5) → 4(1, 4)	<8	0.15[a]	<1.8E12	<9.0E−11
c-C_5H_2	3(1, 3) → 2(1, 2)	<7	0.15[a]	<2.0E12	<1.0E−10
c-C_5H_2	3(0, 3) → 2(0, 2)	<9	0.15[a]	<4.0E12	<2.0E−10
pyrrole	2(0, 2) → 1(0, 1)	<3	0.15[a]	<4.0E11	<2.0E−11
glycine-I.....	3(1, 2) → 2(1, 1)	<3	0.15[a]	<6.0E12	<3.0E−10

NOTE.—These complex carbon species were observed toward R.A.(1950.0) = $04^h38^m41^s0$, decl.(1950.0) = 25°35′40″. X(species) is the abundance relative to H_2, assuming that $N(H_2) = 2.0 \times 10^{22}$ cm^{-2} (Pratap et al. 1997). Upper limits are 3 σ-rms.

[a] Assumed line width for this calculation, consistent with HC_7N, CCS, and C_8H.

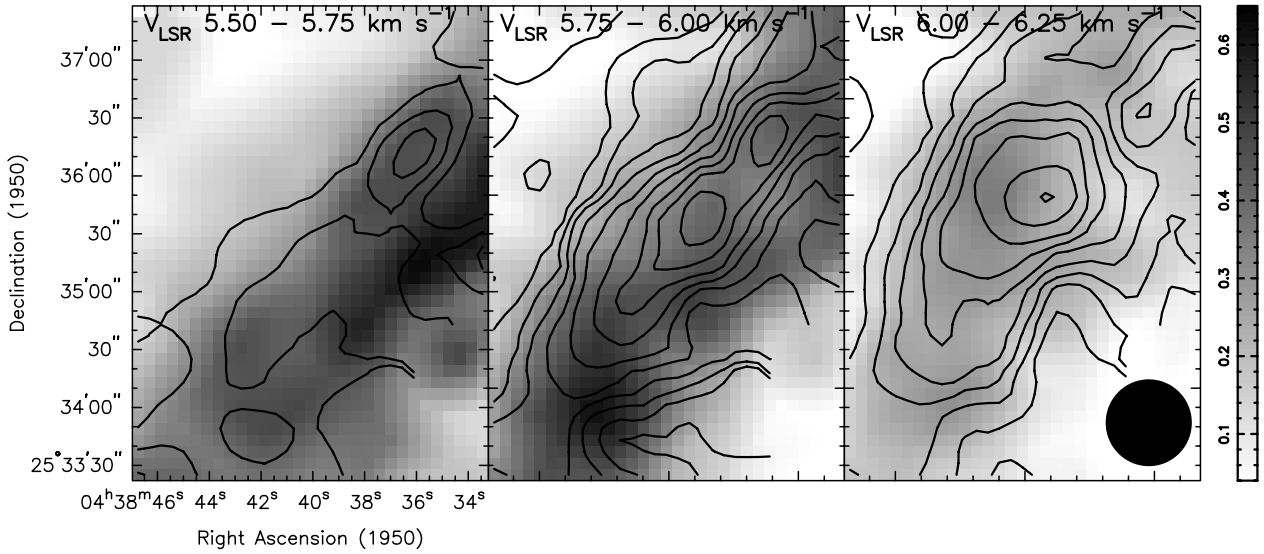

FIG. 3.—Integrated intensity maps of HC_7N (*contour*) and CCS (*gray scale*) for three different velocity intervals. The (0, 0) position for the map is R.A.(1950.0) = $04^h38^m39^s.0$, decl.(1950.0) = 25°35′30″. The beam size is 45″, the map is sampled every 25″ (nearly Nyquist sampled), and the signal-to-noise ratio is much greater than 10 for both species.

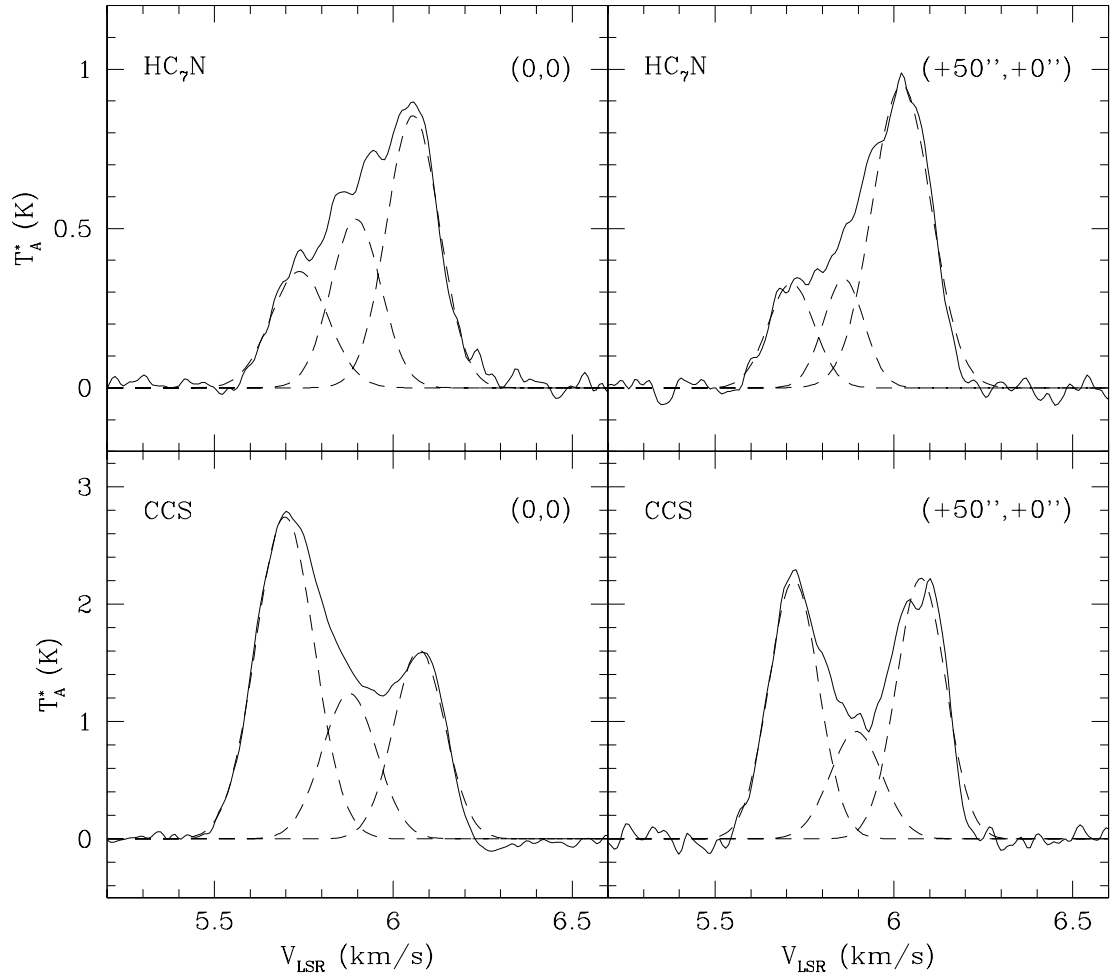

FIG. 4.—Spectra of HC_7N ($J = 20 \rightarrow 19$) and CCS ($J_N = 2_1 \rightarrow 1_0$) in TMC-1 at the (0,0) position [R.A.(1950.0) = $04^h38^m39^s.0$, decl.(1950.0) = 25°35′30″] and (+50″, +0″). The spectral resolution is 0.008 km s^{-1}. The results of the Gaussian decomposition, assuming three velocity components, is shown by the dotted lines.

TABLE 3

GAUSSIAN-FITTED PARAMETERS TO HC_7N AND CCS SPECTRA

Species	T_A^* (K)	ΔV (km s^{-1})	V_{LSR} (km s^{-1})	N(species) (cm^{-2})
		Position (0, 0)		
HC_7N.....	0.37	0.17	5.74	7.6E12
	0.53	0.16	5.90	1.0E13
	0.86	0.17	6.06	1.8E13
CCS.....	2.74	0.19	5.70	3.0E13
	1.24	0.18	5.88	1.1E13
	1.61	0.17	6.07	1.4E13
		Position (+50″, +0″)		
HC_7N.....	0.33	0.15	5.71	5.9E12
	0.34	0.14	5.86	5.8E12
	0.95	0.17	6.02	2.0E13
CCS.....	2.21	0.16	5.72	2.0E13
	0.91	0.17	5.89	7.8E12
	2.22	0.16	6.07	2.0E13

NOTE.—The (0, 0) position corresponds to R.A.(1950.0) = $04^h38^m39^s.0$, decl.(1950.0) = 25°35′30″.

pressure is not a significant support mechanism for these clumps. The fitted LSR velocities agree well for both species too, with central velocities near 5.7, 5.9, and 6.1 km s^{-1} for the three components. The errors in the line width and central velocity are generally less than 0.01 km s^{-1} from the Gaussian fits.

It is quite possible that there are more than three velocity structures in each line of sight. Peng et al. (1998) found convincing evidence for 45 clumps in an 8′ × 8′ region toward TMC-1 core D, previously described by Hirahara et al. (1992). Given the positions and sizes of the Peng cores, we determined that there could be as many as six clumps within our beam contributing to the emission at the (0, 0) position. For simplicity, here we base our discussions on the three–velocity-component model. More components will only strengthen these conclusions.

We estimate column densities for HC_7N and CCS for each of the three velocity components toward the two lines of sight listed in Table 3. In this calculation, we have assumed that the emission is optically thin and that the energy levels are populated according to a Boltzmann distribution at an excitation temperature of 5 K, similar to that found for many complex species in TMC-1 (Pratap et al. 1997). The relationship between integrated intensity and column density used in this calculation is described by Turner (1991). The results are included in Table 3. In general, the S/N is much greater than 10 for HC_7N and CCS. Since the column density uncertainties are proportional to the noise, the uncertainties in this calculation are much less than 10%, and we omit them from further discussions. Note that the abundance ratio [HC_7N]/[CCS] varies by factors of 3–5 within a single beam. The variations seen in the velocity maps (Fig. 3) assure us that such variations are common throughout the cloud, and not just at the positions we have chosen to analyze.

4. DISCUSSION

In the previous section, we presented arguments for chemical variations on size scales of 0.03 pc. The line shapes for a variety of molecular species related by their degree of carbon complexity (§ 3.1) are consistent with the scenario in which distinct clumps in close proximity have different evolutionary status. We quantitatively showed the line-of-sight chemical abundance variations based on the velocity maps of two different species (§ 3.3). We now examine this further in the light of gas-phase chemistry models, while incorporating what we know about the physical conditions of the small-scale clumps in TMC-1 from CCS (Langer et al. 1995; Wolkovitch et al. 1997; Peng et al. 1998).

In purely gas-phase chemical models, both CCS and HC_7N peak at "early" times in the evolution of a core. For the physical conditions appropriate to TMC-1, the CCS abundance rises quickly, peaks at 4×10^4 yr, and falls off by a factor of 5 by 10^6 yr. In contrast, HC_7N increases more gradually, does not peak until 2×10^5 yr, and falls off rather quickly by 8×10^5 yr (K. Willacy 2001, private communication). Thus, within the first 10^5 yr we should see a large CCS abundance without appreciable amounts of HC_7N. Ruffle et al. (1997) and Gwenlan et al. (2000) have argued that a secondary "late-time" abundance peak occurs for cyanopolyynes (such as HC_3N, HC_5N, HC_7N) at $>3 \times 10^6$ yr. Their models deal specifically with HC_3N, but they infer similar characteristics for cyanopolyynes in general. Such late secondary-abundance maxima do not occur for sulfur-bearing species such as CCS. Strong CCS emission toward the lines of sight in TMC-1 suggests that such late-time chemistry is not likely, and that the HC_7N abundance is more indicative of early-time chemistry ($<10^6$ yr) in TMC-1.

For the physical conditions appropriate to TMC-1, chemical models that include the accretion of molecules onto dust (Rawlings et al. 1992; Bergin & Langer 1997) show that gas-phase depletion onto cold (10 K) dust is not effective until after 10^6 yr. These models also show that after the onset of depletion, some species, especially CS and CCS, are preferentially removed from the gas phase earlier in this process than species such as NH_3. L1498 is a classical example demonstrating the success of these models. Observations of L1498 show a dense core traced by NH_3 surrounded by CCS and CS limb-brightened shells (Kuiper et al. 1996). Further observations by Willacy et al. (1998) using continuum data confirmed that the CCS depletion was indeed the result of an increase in the density toward the center of the core, effectively increasing the rate of preferential depletion of CCS onto grains. Based on this observational evidence, we conclude that strong emission from both CCS and HC_7N in TMC-1 is indicative of early-time chemistry ($<10^6$ yr), without the need to include the effects of freeze-out onto grains. Nevertheless, the high degree of clumpiness in TMC-1 may have significant dynamical effects on its chemistry.

In addition to the prevalence of early-time gas-phase chemistry in TMC-1, as pointed out by Markwick et al. (2000), the presence of some of the oxygen-bearing organic molecules such as HCNO, CH_2CO, CH_3CHO, H_2CO, and HC_2CHO indicates that they form in grain surface reactions, as in "hot cores." Markwick et al. (2000) developed a dynamical chemical model for the evolution of the TMC-1 ridge. They identify MHD waves from IRAS 04381+2540 as a mechanism for grain mantle removal, triggered by explosions of radical-rich mantles and by thermal desorption during the passage of these MHD waves. Injection of ice mantles containing simple hydrocarbons enriches the gas phase and can explain some of the organic diversity in TMC-1. MHD waves are quickly dissipated in a dense

medium. In order for the MHD waves to influence the gas at the cyanopolyyne peak (CP, $\sim$0.3 pc away from IRAS 04381+2540), these authors had to invoke an extremely clumpy medium. Only then could this model explain the observed large-scale abundance gradients identified between the CP peak and the NH_3 peak in TMC-1. Our observations, and those of Peng et al. (1998), show direct evidence for such clumpiness, providing support for this model.

We show here that the passage of MHD waves through the clumpy medium, in addition to providing a basis for "hot-core" chemistry, also plays a role in maintaining the early-time chemistry in the clumps by refreshing the gas-phase chemical process. Markwick et al. (2000) suggested that collisions between clumps will provide another source of MHD waves that act over a smaller localized region. We use our estimates of the small-scale abundance gradients in TMC-1 (from the spatial and velocity structure of the HC_7N and CCS gas) to consider the influence of such MHD waves on small scales, driven by clump-clump collisions.

The Alfvén velocity, v_A, is given by $1.3B_{100}n_4^{-1/2}$ km s^{-1} (Zweibel & Josafatsson 1983), where B_{100} is the magnitude of the magnetic field in units of 100 μG and n_4 is the molecular hydrogen density in units of 10^4 cm^{-3}. For typical values of TMC-1, $B_{100} = 1$ and $n_4 = 6$, we find $v_A = 0.5$ km s^{-1}. Such a large value for B_{100} is inferred for the Taurus cloud (Troland et al. 1996), and is significantly less than that obtained by scaling a 30 μG field at $n_4 = 0.1$ to the TMC-1 conditions using the scaling law $B \propto n^{1/2}$. Recall that the distance between the HC_7N and CCS peaks in our map (Fig. 3) is on the order of 0.03 pc. Then, in as little as 6×10^4 yr, we should see evolutionary effects over those distances. This timescale is comparable to the difference in peak abundance times between CCS and HC_7N ($\sim 10^5$ yr) in TMC-1.

The basic scenario discussed here is that two clumps collide and release MHD waves. The resulting clump evolves for approximately 10^5 yr, long enough to form HC_7N. During that time, the MHD wave generated in the collision has encountered a second clump $\sim$0.03 pc away (at 6×10^4 yr), the MHD wave has effectively reset the chemical clock, and the second clump has evolved to form CCS (4×10^4 yr), but this has not been long enough to form significant amounts of HC_7N.

This simple collision-evolution scenario adequately explains the large variations in the [HC_7N]/[CCS] abundance ratio in the line-of-sight calculations. Within a single beam toward two positions, we determine that the abundance ratio [HC_7N]/[CCS] changes by a factor of 3–5 between the lowest and highest velocity gas (Table 3). Within a beam, we are measuring the gas along the line of sight. If we assume that TMC-1 has a cylindrical structure, then two clumps can, at most, be separated by the distance across the ridge, 3′ or 0.12 pc. With at least three and as many as six clumps along our line of sight, we are talking about clump-clump distances of $\sim$0.03 pc, considering their distribution in a three-dimensional volume along the line of sight. This matches our previous estimate of a distance of 0.03 pc over which a 0.5 km s^{-1} Alfvén wave can encounter a second clump and still allow this clump enough time to evolve, forming CCS but not HC_7N.

Propagation of MHD waves from clump-clump collisions alone can trigger small-scale abundance variations and chemical complexity in the neighboring clumps. However, the clump-clump collisions also provide a mechanism capable of raising the mantled dust grains from 10 K to $T_{crit} \sim 30$ K within each colliding clump. Such an increase in the temperature of the grain mantle will induce reactive radical mantle explosions. Consider clump-clump collisions at a velocity comparable to the overall velocity dispersion in the line spectra. Using the relationship (Draine 1985)

$$T_{crit} = 200 \text{ K } (\Delta v/\text{km s}^{-1})^2 , \quad (1)$$

we find that a velocity difference Δv between the colliding clumps of $\sim$0.4 km s^{-1} is sufficient to initiate rapid mantle desorption. The typical line-of-sight velocity difference between clumps in TMC-1 is on the order of 0.2–0.4 km s^{-1}, corresponding to 0.3–0.6 km s^{-1} in space.

The collisions among these clumps occur just at the boundary of the velocity regime ($\lesssim$1 Mach number) for generating weak shocks. The signal speed in the neutral gas is about 0.3–0.5 km s^{-1} for thermal fragments, comparable to the velocity dispersion. Collisions of clumps at velocities comparable to the signal speed correspond to a slow shock in which the gas conditions are little changed across the shock front. Detailed collision models are necessary, however, to follow the evolution of such collisions and determine whether they slow down, accrete, or re-expand. However, for estimating the effect on the grain chemistry, it is only necessary to consider what happens at the collision interface.

The collisions of hydrogen molecules between the incident clump and the target clump occur rapidly at typical clump densities, and the collision time for slowing down the incoming hydrogen by energy transfer is $\tau^s_{H\text{-}H} \sim 0.02(n_4 v_{0.4})^{-1}$ yr, where n_4 is the molecular hydrogen density in units of 10^4 molecules cm^{-3}, and $v_{0.4}$ is the velocity in units of 0.4 km s^{-1}. The much more massive grains, in contrast, transfer much less of their energy in each collision, of the order of m_H/m_{grain} (or about 10^{-10}), so that many collisions are necessary to slow the grain down. The grain-gas slow-down time is of the order of

$$\tau^s_{grain\text{-}gas} \sim 3 \times 10^3 (n_4 v_{0.4})^{-1} a_{0.1}^{-2} \quad \text{yr} , \quad (2)$$

where $a_{0.1}$ is the grain radius in units of 0.1 μm. Thus, the grains travel several orders of magnitude farther into the clump than the gas, but it is still a short distance (10^{15}–10^{16} cm) compared to the clump sizes of order 10^{17} cm. In contrast, the grain-grain collision time between two colliding clumps is comparatively long, of the order of

$$\tau_{gg} \sim 3 \times 10^5 (n_4 v_{0.4})^{-1} a_{0.1}^{-2} \quad \text{yr} \quad (3)$$

for a number density of grains given as $10^{-12} n_{H_2}$.

Comparison of the grain-gas slow-down time with the grain-grain collision time indicates that only about 1%–2% of the grains will undergo collisions of sufficient energy to result in mantle desorption. Whether clump-clump collisions can result in significant energetic grain collisions for the production of molecules needs to be determined by detailed calculations of the process. However, this mechanism offers possibilities for introducing complex grain mantle material into the gas phase during clump collisions, with composition similar to that seen in "hot-core" chemistry, but with smaller fractional abundances.

Thus, the streaming motions of grains relative to each other during clump-clump collisions provides the needed velocity to invoke "hot-core" chemistry near the surface of

these two clumps. Much of this will occur at the collision surface of these small clumps, which remain spatially unresolved in our beam. Note that inside any clumps not involved in clump collisions, the collisions between grains do not lead to an effective desorption mechanism. This is because the individual clumps are thermally supported (at 10 K) with little turbulence, and the nonthermal velocity dispersion within the clump is at most $\sim$ 0.15 km s^{-1} (insufficient, according to eq. [1], to heat the grains).

We have identified two possible additional mechanisms capable of producing the small-scale abundance variations in the southeastern ridge of TMC-1: (1) propagation of MHD waves produced in clump-clump collisions and (2) grain-grain collisions due to colliding clumps. Because of the large distance of this region away from IRAS 04381+2540, it is unlikely that the MHD waves from the IRAS source can be an efficient mechanism. Both the processes involving clump collisions are capable of inducing mantle explosions, and have important implications for the chemical evolution of TMC-1, and presumably other dense clouds. This enrichment of the gas phase enhances the production of complex hydrocarbons and complex organic species. In this manner, the chemistry of TMC-1 could mimic that of "hot cores," regions of high-mass star formation that have enhanced abundances of large organic species, presumably because of the efficient exchange of species formed in the gas phase and on grain mantles. Because of frequent collisions, these clumps in TMC-1 are transient, which could account for the fact that these clumps all exhibit various stages of early-time chemistry. The large number of clumps in various stages of chemical evolution also increases the chances of detecting large molecules, since there is a greater chance of observing at least one clump at the time of the peak abundance for a given species. In addition, the clumpy nature and mantle-driven chemistry could mean that TMC-1 and other clumpy cores with relative motions exhibit a "hot-core"–type chemistry with an abundance of organic species.

An additional chemical process occurring in the passage of MHD waves through cold molecular material is the nonthermal removal of H_2D^+ through ion-neutral drift (Charnley 1998). The ion H_2D^+ is the only source for the production of N_2D^+ and is the primary source for DCO^+. On the other hand, molecules such as DCN, DNC, and C_3HD are formed from deuterated ions, which are less sensitive to destruction by ambipolar diffusion. Hence, observing small deuteration ratios for species such as DCO^+ and N_2D^+, compared to that for DCN, DNC, and C_3HD, would be a distinct chemical signature of the passage of MHD waves in a cloud such as TMC-1, whose kinetic temperature is too low to thermally remove H_2D^+. There are several strong transitions of molecular species related to DCN, namely DC_3N, DC_5N (see Fig. 2), and DC_7N, which can be mapped with the DSN antennas. Determining the D/H ratio for these species, and other more complicated organic species, would be an important test of the effect that MHD waves have on the chemistry in clumpy cores.

5. SUMMARY

We have combined previous data on the clumpy structure of TMC-1 with new spectral data to study the dynamics and evolution of the small-scale cores in this dense cloud. The spectral shapes of a variety of related complex carbon species suggest that the distinct physical structures in TMC-1 have different evolutionary status. New observation of the complex structure and chemistry of these clumps have enabled us to expand previous work on the carbon chemistry in TMC-1.

We report detection of C_8H with a column density of 3×10^{11} cm^{-2}, comparable to the value of 2.2×10^{11} cm^{-2} obtained by Bell et al. (1999). The lack of detection of C_7H suggests that the amount of carbon locked up in longer C_nH chains is not appreciable. Following the detection of H_2C_4 in TMC-1 with an abundance 25 times that predicted by astrochemical models, and of H_2C_6 with an abundance comparable to the models (Langer et al. 1997), we searched for H_2C_5 and c-C_5H_2. This cumulene carbene chain and its longer chain relatives are of great interest for their possible roles as carriers of the diffuse interstellar bands (McCarthy et al. 1997). The larger abundance of c-C_3H_2 relative to its linear counterpart in TMC-1 (Madden et al. 1989) suggests that there might be a larger amount of c-C_5H_2 in the ISM compared to its linear counterpart H_2C_5. None of the H_2C_5 isomer was detected, but the upper limit is comparable to that predicted by the chemistry models for H_2C_5 (without distinguishing between the linear or cyclic isomer).

Our searches for the biogenic species pyrrole and glycine gave column density upper limits of 4×10^{11} and 6×10^{12} cm^{-2}, respectively. The first limit is an order-of-magnitude improvement for pyrrole, and the second is similar to the best measurement for glycine in a solar-type environment. To improve the measurements substantially beyond what we have done for these two species, future searches will require observations achieving sub-mK rms noise levels.

The high degree of clumpiness in TMC-1 provides a favorable scenario in which the clump dynamics becomes important for chemistry. We identify two mechanisms that can explain the small-scale abundance variations in TMC-1. We show that the passage of MHD waves, locally produced by clump-clump collisions, can explain both the early-time and "hot-core" chemistry in TMC-1. The clump-clump collisions themselves can induce mantle explosions at the collision surface of the clumps. Because of the frequent collisions, these clumps are transient, which could account for the fact the these clumps exhibit early-time chemistry as shown by the large variations in the $[HC_7N]/[CCS]$ abundance ratios on small scales (on the order of the clump-clump distance $\sim$0.03 pc) over timescales of 10^5 yr. Before much chemical evolution can occur, these clumps collide and further enrich the chemistry inside the clumps by induced mantle explosions and thermal desorption.

The authors are grateful for the assistance given by the NASA/DSN 70 m antenna staff during the observations. We also appreciate the many helpful discussions with Karen Willacy regarding the chemistry of dense cores. We would also like to thank Steve Charnley for making several suggestions which greatly improved the discussion. This research was conducted at the Jet Propulsion Laboratory, California Institute of Technology, under support from the National Aeronautics and Space Administration. This work was performed while J. E. D. held a National Research Council-JPL Research Associateship.

REFERENCES

Bell, M. B., Feldman, P. A., Watson, J. K. G., McCarthy, M. C., Travers, M. J., Gottlieb, C. A., & Thaddeus, P. 1999, ApJ, 518, 740
Bergin, E. A., & Langer, W. D. 1997, ApJ, 486, 316
Bergin, E. A., Snell, R. L., & Goldsmith, P. F. 1996, ApJ, 460, 343
Caselli, P., Walmsley, C. M., Tafalla, M., Dore, L., & Myers, P. C. 1999, ApJ, 523, L165
Ceccarelli, C., Loinard, L., Castets, A., Faure, A., & Lefloch, B. 2000, A&A, 362, 1122
Charnley, S. B. 1998, MNRAS, 298, L25
Cronin, J. R., & Chang, S. 1993, in The Chemistry of Life's Origins, ed. J. M. Greenberg et al. (Boston: Kluwer), 209
van Dishoeck, E., Blake, G. A., Draine, B. T., & Lunine, J. I. 1993, in Protostars and Planets III, ed. E. H. Levy & J. I. Lunine (Tucson: Univ. Arizona Press), 163
Draine, B. T. 1985, in Protostars and Planets II, ed. D. C. Black & M. S. Matthews (Tucson: Univ. Arizona Press), 634
Gwenlan, C., Ruffle, D. P., Viti, S., Hartquist, T. W., & Williams, D. A. 2000, A&A, 354, 1127
Hirahara, Y., Suzuki, H., Yamamoto, S., Kawaguchi, K., Kaifu, N., Ohishi, M., Takano, S., Ishikawa, S., & Masuda, A. 1992, ApJ, 394, 539
Kuiper, T. B. H., Langer, W. D., & Velusamy, T. 1996, ApJ, 468, 761
Kutner, M. L., Machnik, D. E., Tucker, K. D., & Dickman, R. L. 1980, ApJ, 242, 541
Langer, W. D., Velusamy, T., Kuiper, T. B. H., Levin, S., Olsen, E., & Migenes, V. 1995, ApJ, 453, 293
Langer, W. D., Velusamy, T., Kuiper, T. B. H., Peng, R., McCarthy, M. C., Travers, M. J., Kovacs, A., Gottlieb, C. A., & Thaddeus, P. 1997, ApJ, 480, L63
Lefloch, B., Castets, A., Cernicharo, J., Langer, W. D., & Zylka, R. 1998, A&A, 334, 269
Madden, S. C., Irvine, W. M., Swade, D. A., Matthews, H. E., & Friberg, P. 1989, AJ, 97, 1403
Markwick, A. J., Millar, T. J., & Charnley, S. B. 2000, ApJ, 535, 256
McCarthy, M. C., Travers, M. J., Kovacs, A., Gottlieb, C. A., & Thaddeus, P. 1997, ApJS, 113, 105
Mezger, P. G., Sievers, A., Zylka, R., Haslam, C. G. T., Kreysa, E., & Lemke, R. 1992, A&A, 265, 743
Myers, P. C., Thaddeus, P., & Linke, R. A. 1980, ApJ, 241, 155
Ohashi, N., Lee, S. W., Wilner, D. J., & Hayashi, M. 1999, ApJ, 518, L41
Olano, C. A., Walmsley, C. M., & Wilson, T. J. 1988, A&A, 196, 194
Peng, R., Langer, W. D., Velusamy, T., Kuiper, T. B. H., & Levin, S. 1998, ApJ, 497, 842
Pratap, P., Dickens, J. E., Snell, R. L., Miralles, M. P., Bergin, E. A., Irvine, W. M., & Schloerb, F. P. 1997, ApJ, 486, 862
Rawlings, J. M. C., Hartquist, T. W., Menten, K. M., & Williams, D. A. 1992, MNRAS, 255, 471
Ruffle, D. P., Hartquist, T. W., Taylor, S. D., & Williams, D. A. 1997, MNRAS, 291, 235
Troland, T. H., Crutcher, R. M., Goodman, A. A., Heiles, C., Kazes, I., & Myers, P. C. 1996, ApJ, 471, 302
Turner, B. E. 1991, ApJS, 76, 617
Velusamy, T., & Langer, W. D. 1998, BAAS, 193, 71.07
Velusamy, T., Langer, W. D., & Levin, S. 1998, in Proc. 6th Symp. on Chemical Evolution and the Origin and Evolution of Life, ed. S. E. Acevedo, D. L. DeVincenzi, & S. Chang (Washington, D.C.: NASA), 63
Willacy, K., Langer, W. D., & Velusamy, T. 1998, ApJ, 507, L171
Wolkovitch, D., Langer, W. D., Goldsmith, P. F., & Heyer, M. 1997, ApJ, 477, 241
Zweibel, E. G., & Josafatsson, K. 1983, ApJ, 270, 511